Check for updates

The effects of inflammation on connexin 43 in chronic Chagas disease cardiomyopathy

Breno Cardim Barreto[1,2,3], Maria Vitória Gomes das Neves[1,2],
Carine Machado Azevedo Cardoso[1], Cássio Santana Meira[1,3],
Pâmela Santana Daltro[2], Cláudio Pereira Figueira[1],
Girlaine Café Santos[1,2], Daniela Nascimento Silva[3],
Fábio Távora[4], João David de Souza Neto[4],
Simone Garcia Macambira[1,2], Paul D. Lampe[5],
Keyla Cristiny da Silva Coutinho[6], Tais Hanae Kasai Brunswick[6],
Ricardo Ribeiro dos Santos[1,3†],
Antônio Carlos Campos de Carvalho[6]
and Milena Botelho Pereira Soares[1,3*]

[1]Gonçalo Moniz Institute, Oswaldo Cruz Foundation (IGM-FIOCRUZ/BA), Salvador, Brazil,
[2]Department of Biochemistry and Biophysics, Federal University of Bahia (UFBA), Salvador,
Bahia, Brazil, [3]SENAI Institute of Innovation in Health Advanced Systems (CIMATEC ISI SAS), University
Center SENAI/CIMATEC, Salvador, Bahia, Brazil, [4]Messejana Heart and Lung Hospital, Fortaleza, Brazil,
[5]Translational Research Program, Fred Hutchinson Cancer Center, Seattle, WA, United States,
[6]Biophysics Institute Carlos Chagas Filho, Federal University of Rio de Janeiro, Rio de Janeiro, Brazil

Background: Cardiac arrhythmias are the main cause of sudden death due to Chronic Chagasic Cardiomyopathy (CCC). Here we investigated alterations in connexin 43 (Cx43) expression and phosphorylation in cardiomyocytes as well as associations with cardiac arrhythmias in CCC.

Methods: C57Bl/6 mice infected with *Trypanosoma cruzi* underwent cardiac evaluations at 6 and 12 months after infection via treadmill testing and EKG. Histopathology, cytokine gene expression, and distribution of total Cx43 and its phosphorylated forms Cx43^{S368} and Cx43$^{S325/328/330}$ were investigated. Human heart samples obtained from subjects with CCC were submitted to immunofluorescence analysis. *In vitro* simulation of a pro-inflammatory microenvironment (IL-1β, TNF, and IFN-γ) was performed in H9c2 cells and iPSC-derived cardiomyocytes to evaluate Cx43 distribution, action potential duration, and Lucifer Yellow dye transfer.

Results: Mice chronically infected with *T. cruzi* exhibited impaired cardiac function associated with increased inflammation, fibrosis and upregulated IL-1β, TNF, and IFN-γ gene expression. Confocal microscopy revealed altered total Cx43, Cx43^{S368} and Cx43$^{S325/328/330}$ localization and phosphorylation patterns in CCC, with dispersed staining outside the intercalated disc areas, i.e., in lateral membranes and the cytoplasm. Reduced co-localization of total Cx43 and N-cadherin was observed in the intercalated discs of CCC mouse hearts compared to controls. Similar results were obtained in human CCC heart samples, which showed Cx43 distribution outside the intercalated discs. Stimulation of human iPSC-derived cardiomyocytes or H9c2 cells with IL-1β, TNF, and IFN-γ induced

alterations in Cx43 localization, reduced action potential duration and dye transfer between adjacent cells.

Conclusion: Heart inflammation in CCC affects the distribution and phosphorylation pattern of Cx43, which may contribute to the generation of conduction disturbances in Chagas disease.

Introduction

Considered by the World Health Organization (WHO) to be both a neglected disease and a major public health problem, Chagas disease, caused by the protozoan *Trypanosoma cruzi*, is endemic to Latin America and present mainly in low-income regions [1]. Due to the migration of infected individuals to other regions of the world for socioeconomic reasons [2], the disease has also spread to other continents. Currently, it is estimated that 25,000 people acquire the disease annually, and approximately 10,000 people die worldwide each year due to Chagas disease [1].

The course of disease begins with an acute phase, which corresponds to the onset of infection and parasite spread throughout the body, while the chronic phase mainly affects the digestive system and/or the heart [3]. Chronic Chagasic Cardiomyopathy (CCC), the most common clinical manifestation of Chagas disease, displays high morbidity and mortality [4], with cardiac arrhythmias being the main cause of sudden death in affected patients [5, 6].

Cardiac arrhythmias have been associated with alterations in the function and distribution of connexin 43 (Cx43) in cardiac cells [7]. Cx43 is the main protein responsible for forming gap junction channels located in the intercalated discs between adjacent cardiac cells [8]. Gap junctions play an important role in synchronizing rhythmic contractions and the maintenance of cardiac homeostasis through the exchange of small metabolites [9]. Previous studies demonstrated that cardiomyocytes infected by *T. cruzi* present impaired cell-cell communication due to reduced Cx43 expression [9–12]. Alterations in Cx43 have also been observed in arrhythmogenic cardiac diseases of other etiologies, such as ischemic and bacterial myocarditis [13–15].

The precise regulation of gap junctions is crucial for cell-cell communication and the proper propagation of electrical signals between cardiomyocytes. The phosphorylation of Cx43 is critical for regulating Cx43 activity, as well as this protein's lifespan, structure, and localization [7]. Among the phosphorylation sites, serines 368 (S368) and the triplet 325/328/330 (S325/328/330) have been well investigated, demonstrating their role in the regulation of Cx43 function [13, 15, 16]. While Cx43^{S368} is involved in gap junction inactivation and disassembly, which contributes to the electrical uncoupling of cardiomyocytes, Cx43$^{S325/328/330}$ has been associated with gap junction assembly [13, 16–18].

The importance of Cx43 to proper electrical activity in the heart, coupled with the fact that no specific treatments exist for CCC, highlights the need to further our understanding of the role played by Cx43 alterations and investigate relevant relationships with arrhythmias in Chagas disease. Therefore, the present study aimed to evaluate the expression and distribution of total Cx43, as well as its phosphorylated forms, in mice and the hearts of CCC patients. Additionally, we performed an *in vitro* investigation into the role of the pro-inflammatory chagasic microenvironment in Cx43 expression.

Materials and methods

Animals

Four-week-old male C57BL/6 mice were used for *T. cruzi* infection and as uninfected controls. All animals were obtained from the animal care facilities of the Biotechnology and Cell Therapy Center, São Rafael Hospital (CBTC-HSR), and the Gonçalo Moniz Institute, Oswaldo Cruz Foundation (IGM-FIOCRUZ), and kept at room temperature (20 ± 2°C) under controlled humidity (50%) conditions. Food and water were provided *ad libitum* and all animals were exposed to constant 12-hour light-dark cycles. All procedures were approved by the Animal Use Ethics Committee of the São Rafael Hospital (Protocol 011/18) and the Gonçalo Moniz Institute (Protocol 17/2017).

Trypanosoma cruzi infection and experimental design

Mice were infected by intraperitoneal (i.p) injection of saline solution (100 μL) containing 10^3 trypomastigotes of *T. cruzi* (Colombian strain), obtained from cultures of LCC-MK2 cells previously infected with *T. cruzi*. Parasitemia was assessed at

different time points after infection using a standard protocol [19]. All animals were evaluated for cardiac function (exercise testing and electrocardiogram) at 6 or 12 months after *T. cruzi* infection to compare groups of uninfected (n=10) and infected animals (n = 15) at each infection time. Following these evaluations, animals were euthanized using xylazine (50 mg/kg) and ketamine (100 mg/kg) via intraperitoneal, and murine hearts were collected to perform histopathological and immunofluorescence analysis, evaluate gene expression, and undergo transmission electron microscopy (Supplementary Figure S1).

Treadmill testing

Exercise performance was evaluated by placing each mouse on a treadmill in a chamber (LE 8700; Panlab, Barcelona, Spain). Treadmill speed and shock intensity (mA) were controlled by potentiometer (LE 8700-treadmill control, Panlab). The initial speed was 6 cm/s, with increases of 6 cm/s every five minutes until reaching exhaustion. Exhaustion was considered following an animal's permanence for a period of 10 seconds on the electrified stainless-steel grid that served as a stimulus to perform the activity. The parameters evaluated were walking distance and total exercise time [20].

Electrocardiographic analysis

Mice were submitted to inhalational anesthesia with isoflurane (0.5 to 2%) to acquire electrocardiographic data. Electrocardiographic (EKG) records were obtained using the BioAmp Powerlab system (PowerLab 2\20, ADInstruments, Castle Hill, NSW, Australia) via bipolar leads I and II. The obtained data was then analyzed using LabChart7 software (PowerLab), applying filters in the range of 1 to 100 Hz to minimize environmental signal disturbances, with a sampling rate of 1 kHz. The parameters evaluated on EKG included heart rate, PR interval, P wave duration, QT interval, corrected QT interval (QTc), and the presence of arrhythmia. Wave durations (ms) and heart rate were automatically calculated by the software. QTc was calculated as the ratio of the QT interval to the square root of the RR interval (Bazett's formula) [20, 21].

Histopathological and morphometric analyses

Following euthanasia, murine heart samples were fixed in 4% formalin for paraffinization and the preparation of histological sections. The quantification of inflammatory cells and the percentage of fibrotic tissue were performed on slides under bright field microscopy following staining with hematoxylin-eosin (H&E) and Sirius red, respectively. Images were captured using a CoolSnap digital camera adapted to an AX-70 microscope (Olympus) and analyzed using Image-Pro Plus software, version 5.0 (Media Cybernetics). To quantify the number of inflammatory

infiltrate cells, 5 fields/animal were captured from HE-stained slides at 400x magnification. The extent of fibrosis was estimated in Sirius red-stained heart sections using the same program by comparing areas of fibrotic and non-fibrotic tissue in 10 fields per animal at 200x magnification [21]. The micrography analyses were done blinded.

Gene expression analysis by RT-qPCR

RNA was extracted from murine heart tissue using TRIzol reagent (Invitrogen, Carlsbad, CA), with concentrations determined by photometric measurement. A High-Capacity cDNA Reverse Transcription Kit (Applied Biosystems, Foster City, CA) was used to synthesize cDNA from 1 μg of RNA in accordance with the manufacturer's recommendations. cDNA synthesis and RNA expression analysis were performed by Real-Time PCR using TaqMan Gene Expression Assays for *Gja1* (Mm00439105_m1), *Tnf* (Mm00443258_m1), *Il1b* (Mm0043228_m1) and *Ifng* (Mm01168134_m1). All reactions were run in duplicate on an ABI 7500 Real Time PCR System (Applied Biosystems) under standard thermal cycling conditions. A non-template control (NTC) and non-reverse transcription controls (No-RT) were also included. Samples were normalized with *Hprt* (endogenous control). The threshold cycle (2-ΔΔCt) method of comparative PCR was used to analyze the obtained results [22].

Human heart samples

Tissue samples of explanted hearts were obtained from the heart transplant service of Hospital de Messejana in Fortaleza (Ceará-Brazil). Left ventricular sections were obtained from the explanted hearts of patients with CCC (n = 3). As a control, a sample was obtained from the heart of a patient without cardiomyopathy who died from stomach cancer (n = 1) (Supplementary Table S1). Sections were processed and then subsequently subjected to immunofluorescence analysis. The local institutional review board of the Hospital de Messejana approved the present study protocol (Approval number: 3.255.044).

Cardiac tissue immunofluorescence

Sections of paraffin-embedded hearts fixed in formalin were used to detect the expression and distribution of total Cx43, as well as phosphorylated Cx43^{S368} and Cx43$^{S325/328/330}$ by immunofluorescence. Heart sections were incubated overnight with anti-total Cx43 (1:50; Santa Cruz Biotechnology, Santa Cruz, CA; SC-9059), anti-Cx43^{S368} (1:100; Thermo Fisher Scientific; 48-3000), anti-Cx43$^{S325/328/330}$ (1:2000) [23] and N-cadherin (1:100; Thermo Fisher Scientific; 33-3900) antibodies, at 4°C. Next, secondary anti-rabbit IgG AlexaFluor 488 conjugated antibody (1:1000; Life Technologies; A21441) and Wheat Germ Agglutinin (1:1000; WGA - AlexaFluor 594; W11262), or anti-mouse IgG

AlexaFluor 568 conjugated (1:1000; Life Technologies, A10037) were added, followed by a 1-hour incubation period at room temperature. Slides were mounted using Vectashield mounting medium with DAPI (Vector Laboratories). Images were obtained using a TCS SP8 spectral confocal microscope (Leica) and analyzed using ImagePro version 7.0 software (Media Cybernetics). The micrography analyses were done blinded.

Transmission electron microscopy – immunogold labeling

Left ventricle heart fragments obtained from infected and healthy mice were fixed using a solution containing glutaraldehyde (1%), paraformaldehyde (4%), picric acid (0.2%), and 0.1 M sodium cacodylate for at least 3 h at 4°C. After fixation, the fragments were processed as previously described for inclusion in LR-White resin (24). Next, ultra-thin sections were obtained and transferred to collodion-coated nickel gratings. Grids were blocked with 50 mM glycine, 10% BSA (Aurion, Wageningen, Netherlands) and 0.1% Tween 20 (Sigma-Aldrich, Hamburg, Germany) for 30 minutes each. After blocking, the grids were incubated overnight at 4°C with primary anti-connexin antibody 43 (1:10; Santa Cruz Biotechnology), and then for 1 h with secondary goat anti-rabbit antibody conjugated to colloidal gold (10 nm) (1:100; Sigma-Aldrich; G7-402). For negative controls, grids were incubated in 0.1 M phosphate-buffered saline (PBS) instead of the primary antibody. All grids were finally stained with uranyl acetate and lead citrate, and subsequently examined under a JEOL TEM-1230 transmission electron microscope operating at 80Kv. The micrography analyses were done blinded.

H9c2 cell cultures

H9c2 cells, initially isolated from an embryonic BD1X rat heart, were used to analyze Cx43 expression in vitro (25). H9c2 cells were cultured in Dulbecco's modified Eagle's medium (DMEM; Life Technologies, GIBCO-BRL, Gaithersburg, MD) supplemented with 10% fetal bovine serum (FBS; GIBCO) and 50 μg/mL of gentamicin (Life Technologies), maintained at 37°C under a humidified atmosphere of 5% CO_2, with the culture medium changed every two days until reaching 80%-90% confluence.

H9c2 cells were plated at a density of 5×10^5 cells per well on 24-well plates containing glass coverslips. Following cell adherence to the coverslips, cultures were stimulated with a combination of pro-inflammatory cytokines (IL-1β, TNF, and IFN-γ; 10 ng/ml of each cytokine; Cell Signaling Technology) (26, 27) in DMEM supplemented with 10% FBS for 48 h. Glass coverslips containing H9c2 cells were then washed with PBS and fixed in 4% paraformaldehyde (Thermo Scientific, Wilmington, DE) for 15 minutes at room temperature. The cells were washed again with PBS and nonspecific sites were blocked with PBS plus 5% BSA for 30 minutes and then incubated overnight at 4°C with the primary antibody, anti-total Cx43 (1:100; Santa Cruz Biotechnology). Next, the cells were washed with PBS-Tween and PBS 1x and incubated

with the secondary anti-rabbit IgG antibody (AlexaFluor 488; 1:400) and Wheat Germ Agglutinin (WGA – AlexaFluor 594; 1:1000) diluted in PBS plus 1% BSA. Slides were mounted using Fluoroshield mounting medium with DAPI (Sigma-Aldrich). Images were obtained using a TCS SP8 spectral confocal microscope (Leica), with fluorescence intensity evaluated using ImagePro software version 7.0 (Media Cybernetics).

Dye transfer analysis

The functional assessment of gap junctions was carried out through in vitro dye transfer analysis. Firstly, H9c2 cells cultivated on 24-well plates at a density of 5×10^5 cells/well were stimulated with pro-inflammatory cytokines for 48h. Incisions through monolayers were performed with the tip of a scalpel in the presence of Lucifer Yellow (LY) dye (Sigma-Aldrich) for 5 minutes. Next, cells were washed three times with PBS containing Ca^{2+} and Mg^{2+} to remove excess dye, and then fixed in 10% formaldehyde for 15 minutes at room temperature (28). Images were obtained using a ZOE Fluorescent Cell Imager (BioRad).

Cardiomyocyte action potential and immunofluorescence analysis

Induced pluripotency stem cell (iPSC)-derived cardiomyocytes, originally collected from healthy donor, were obtained from the Laboratory of Cellular and Molecular Cardiology, Federal University of Rio de Janeiro (UFRJ) (29). iPSCs were cultured in RPMI medium (LGC Biotecnologia) supplemented with B-27 (GIBCO) without insulin. Activation of the Wnt pathway was performed by treatment with CHIR99021(9 μM), a glycogen synthase kinase 3 (GSK3) inhibitor (R&D Systems), on day 0 (D0). Subsequently, the Wnt pathway was inhibited by treatment with the antagonist XAV939 (R&D Systems) at concentrations of 10 and 5 μM, respectively on days 3 and 4 (D3 and D4). After this step, from D7 onwards, the medium initially used was replaced by medium containing insulin and RPMI/B-27 Plus, which was regularly changed every two days until complete cardiomyocyte maturation was achieved on D30. This protocol was adapted from Lian et al. (2013). The cell line Pac25 used in this work was obtained from a healthy donor was previously approved by a national ethical review board in Brazil (CONEP: # 409960/2013-6; CEP: 63167722.0.0000.5272).

Next, iPS-derived cardiomyocytes were characterized by flow cytometry. Cells were fixed and permeabilized with BD Cytofix/Cytoperm™ (BD Biosciences) and stained with pluripotency markers OCT3/4 (1:100; BD Biosciences), SOX2 (1:100; BD Biosciences), and cardiac marker Troponin T (1:100; Thermo-Fisher). (Supplementary Figure S2) (29).

Human iPSC-derived cardiomyocytes (3×10^5 cells) were plated in 35 mm culture dishes in RPMI/B-27 Plus in the absence or presence of recombinant IL-1β, TNF, and IFN-γ (10 ng/ml of each cytokine) to induce an in vitro inflammatory microenvironment. After 24 or 48 h, cultures were used for electrophysiology analysis.

Cells were continuously perfused with a Tyrode solution containing (in mM) 140 NaCl, 5.4 KCl, 1.8 CaCl2, 1.0 MgCl2, 11 D-glucose and 10 HEPES, at pH 7.4 under a constant temperature of 37°C.

Action potential was recorded using a glass microelectrode with a resistance of 40-100 MΩ (1.5 x 0.86 mm – P-97 Flaming/Brown Micropipette Puller – Sutter Instrument), filled with KCl solution (3 M) and connected to a signal amplifier (MultiClamp 700B, Molecular Devices, USA). The amplified signal was digitized (DIGIDATA 1440 A/D interface, Axon Instrument, Inc.) and the obtained data was analyzed using LabChart 7.3 software (ADInstruments, Australia). Action potential duration (APD) was analyzed at 10, 50, and 90% of repolarization, considering at least five action potentials from each group.

In addition, human iPSC-derived cardiomyocytes were also used for immunofluorescence analysis. iPSC-derived cardiomyocytes were washed with PBS following the same protocol described above for H9c2 cells. By contrast, these cells were incubated overnight at 4°C with the primary antibody anti-total Cx43 (1:100; Santa Cruz Biotechnology) diluted in PBS containing 1% BSA. Next, the cells were washed with PBS-Tween and PBS 1x and incubated with the secondary anti-rabbit antibody (AlexaFluor 568; 1:800) and phalloidin (AlexaFluor 488; 1:400) for 1 hour at room temperature. Slides were mounted using Fluoroshield mounting medium with DAPI (Sigma-Aldrich).

Statistical analysis

Data are expressed as means ± standard error of the mean for the number of animals in each group. The normal distribution of data was confirmed by the Shapiro-Wilk test Student's t test was used to compare quantitative variables between groups at a given timepoint. For comparisons between three groups, data were analyzed using one-way ANOVA, followed by the Newman-Keuls multiple comparison test. Significant differences were considered for p values below 0.05. All analyses were performed using Graph Pad Prism version 8.0 (Graph Pad Software, San Diego, CA).

Results

Chronic infection with *T. cruzi* reduces treadmill performance, promotes cardiac arrhythmias, inflammation and fibrosis

The cardiac function of mice with CCC was evaluated at 6 and 12 months after infection. The treadmill performance of *T. cruzi*-infected mice was significantly impaired ($P < 0.001$) compared to uninfected control littermates, which run greater distances (Figure 1A) for longer times of exercise (Figure 1B) at both times after infection. Additionally, EKG analysis revealed that *T. cruzi*-infected mice present severe cardiac conduction disturbances (Figures 1C–E). The alterations identified correspond to different types of arrhythmias, including polymorphic ventricular tachycardia, junctional rhythm, atrioventricular dissociation, and atrioventricular block. By contrast, uninfected control animals presented normal sinus rhythm. No

significant differences were observed in the severity of arrhythmias presented by *T. cruzi*-infected mice when comparing 6 versus 12 months after infection (Figure 1).

Heart sections prepared from the left ventricles were stained with H&E or Sirius red for morphometric analysis of inflammation and fibrosis, respectively. An intense multifocal inflammatory infiltrate predominantly composed of mononuclear cells was found in the heart sections from *T. cruzi*-infected mice (at both 6 and 12 months). The number of inflammatory cells was significantly higher compared to uninfected controls (Figures 2A–C). Collagen deposition analysis indicated a greater area of fibrosis deposition in the cardiac sections of infected mice compared to controls at both time points evaluated (Figures 2D–F). Moreover, increased expression of genes encoding for the pro-inflammatory cytokines TNF, IL-1β, and IFN-γ was detected in heart samples obtained from the infected group compared to uninfected controls 6 or 12 months after infection (Figures 2G–I).

Cardiac Cx43 gene expression, cell distribution, and phosphorylation patterns are affected by *T. cruzi* infection

To evaluate Cx43 gene expression, the left ventricles of mouse hearts were analyzed at 6 and 12 months after *T. cruzi* infection. The expression of *Gja1*, which encodes Cx43, was reduced in the hearts of chagasic mice compared to naïve mice at 6 months, but not at 12 months after infection (Figure 2J).

Next, the distribution of total Cx43 ($Cx43^T$) and its phosphorylated forms ($Cx43^{S368}$ and $Cx43^{S325/328/330}$) were evaluated by confocal microscopy in the left ventricles. The pattern of $Cx43^T$ localization was significantly altered in *T. cruzi*-infected mice compared to uninfected animals. While predominantly located in the intercalated discs in the cardiac sections of uninfected control mice (Figure 3A), in chagasic hearts $Cx43^T$ was frequently identified outside the intercalated discs, appearing in the lateral membrane and scattered into the cytoplasm (Figure 3B). Similar results were observed in heart sections stained with antibodies against phosphorylated Cx43, as $Cx43^{S368}$ and $Cx43^{S325/328/330}$ were detected in the lateral membrane and within the cytoplasm in infected mice compared to uninfected mice, in which Cx43 was mostly restricted to intercalated discs (Figures 3C–F).

Confocal microscopy analysis of heart sections co-stained with anti-$Cx43^T$ and anti-N-cadherin antibodies also indicated alterations induced by chronic *T. cruzi* infection. In the hearts of uninfected animals, staining for these two proteins revealed the localization of both N-cadherin and $Cx43^T$ in the intercalated discs (Figures 4A, B). In contrast, staining for Cx43 was weaker in the intercalated discs in chagasic mice areas, with N-cadherin almost exclusively detected in some areas. $Cx43^T$ staining was often observed in areas adjacent to the intercalated disks, and also scattered into the cytoplasm as well as into lateral membranes (Figures 4C, D).

Next, we performed ultrastructural analysis to evaluate $Cx43^T$ distribution by immunogold labeling using transmission electron microscopy in fragments of murine left ventricles. Heart samples from uninfected mice showed $Cx43^T$ localized in the interplicate
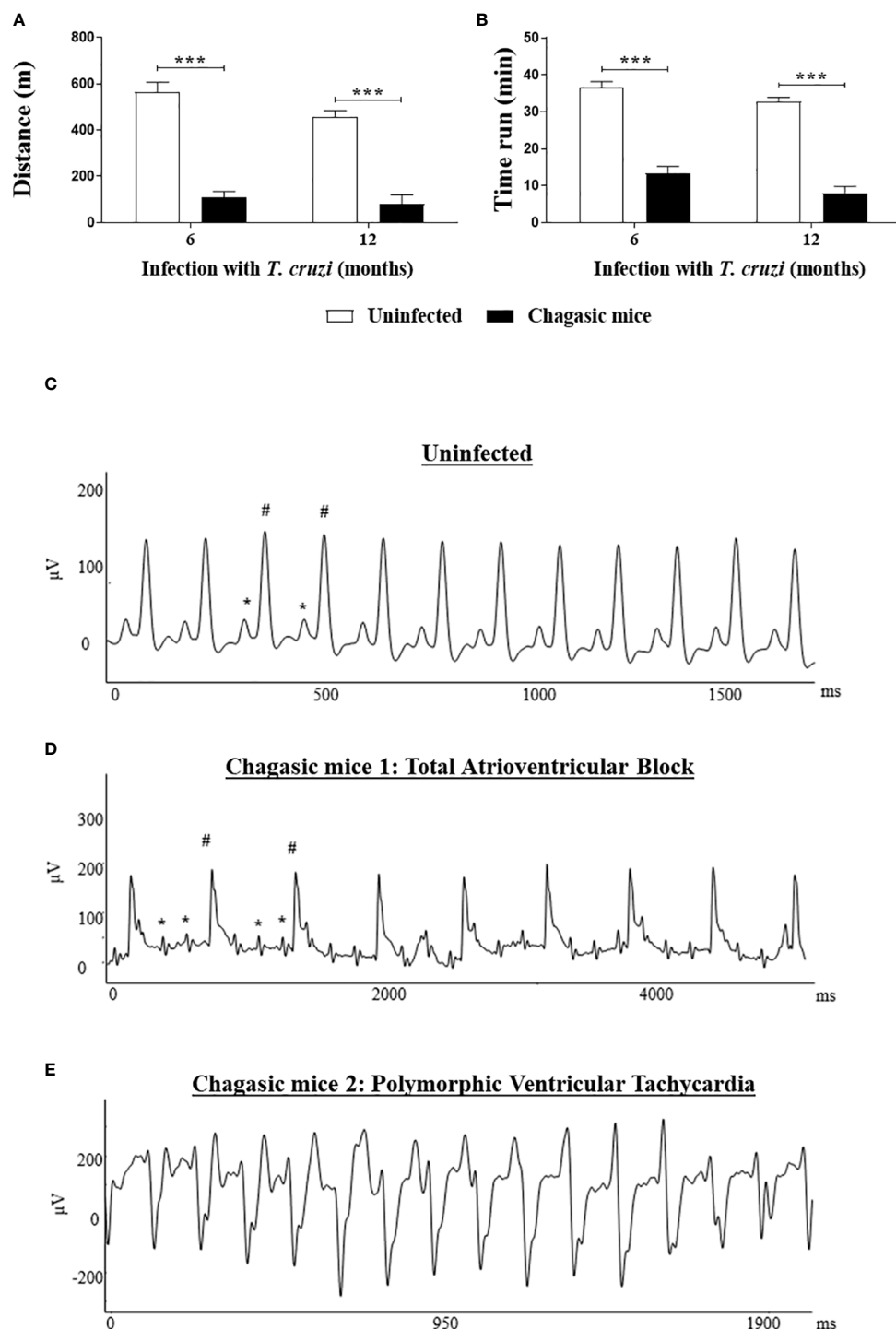
FIGURE 1

Functional analysis: Treadmill testing and EKG analysis of chagasic and uninfected mice. **(A, B)** Distance run and time of exercise on a motorized treadmill involving mice after 6 and 12 months of infection, respectively; Representative EKG images: **(C)** EKG of an uninfected mouse with regular sinus rhythm; **(D)** EKG of a chagasic mouse with total atrioventricular block; **(E)** EKG of chagasic mouse with polymorphic ventricular tachycardia. * = P wave; # = QRS complex. Treadmill test: Values represent means $\pm$ S.E.M. of 10 and 14 mice (6 months of infection) and 7 and 8 mice (12 months of infection) from uninfected and chagasic groups, respectively. ***$P< 0.001$ compared to uninfected group.

regions of cardiomyocyte intercalated discs, adjacent to plicate areas containing loops and desmosomes (Figures 5A–C). The hearts of chronic chagasic mice also showed staining for $Cx43^{T}$ in interplicate regions (Figures 5D–F), as well as in invaginations adjacent to the intercalated discs (Figure 5).

Cell distribution of Cx43 is altered in human chagasic hearts

Samples of cardiac ventricles from patients with heart failure due to chronic Chagas disease who underwent heart transplantation
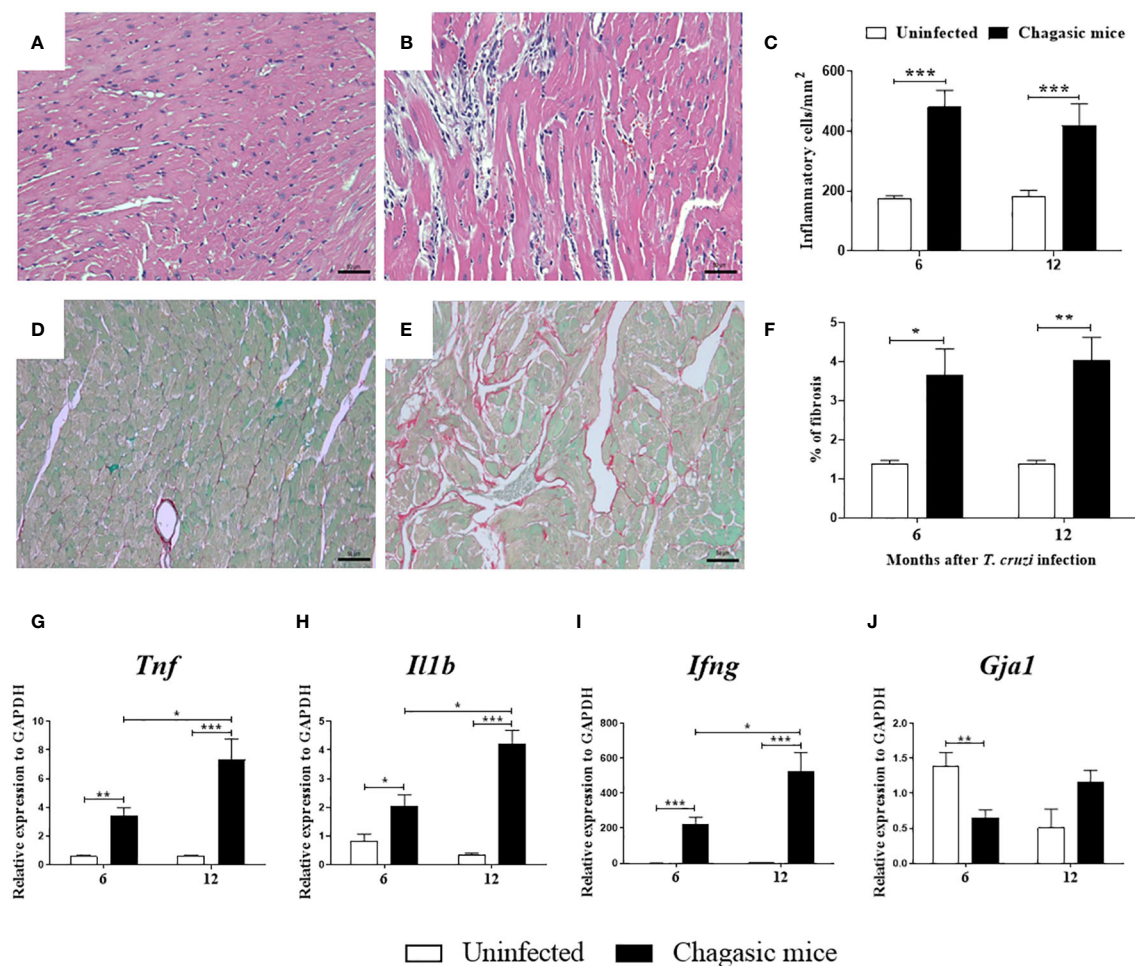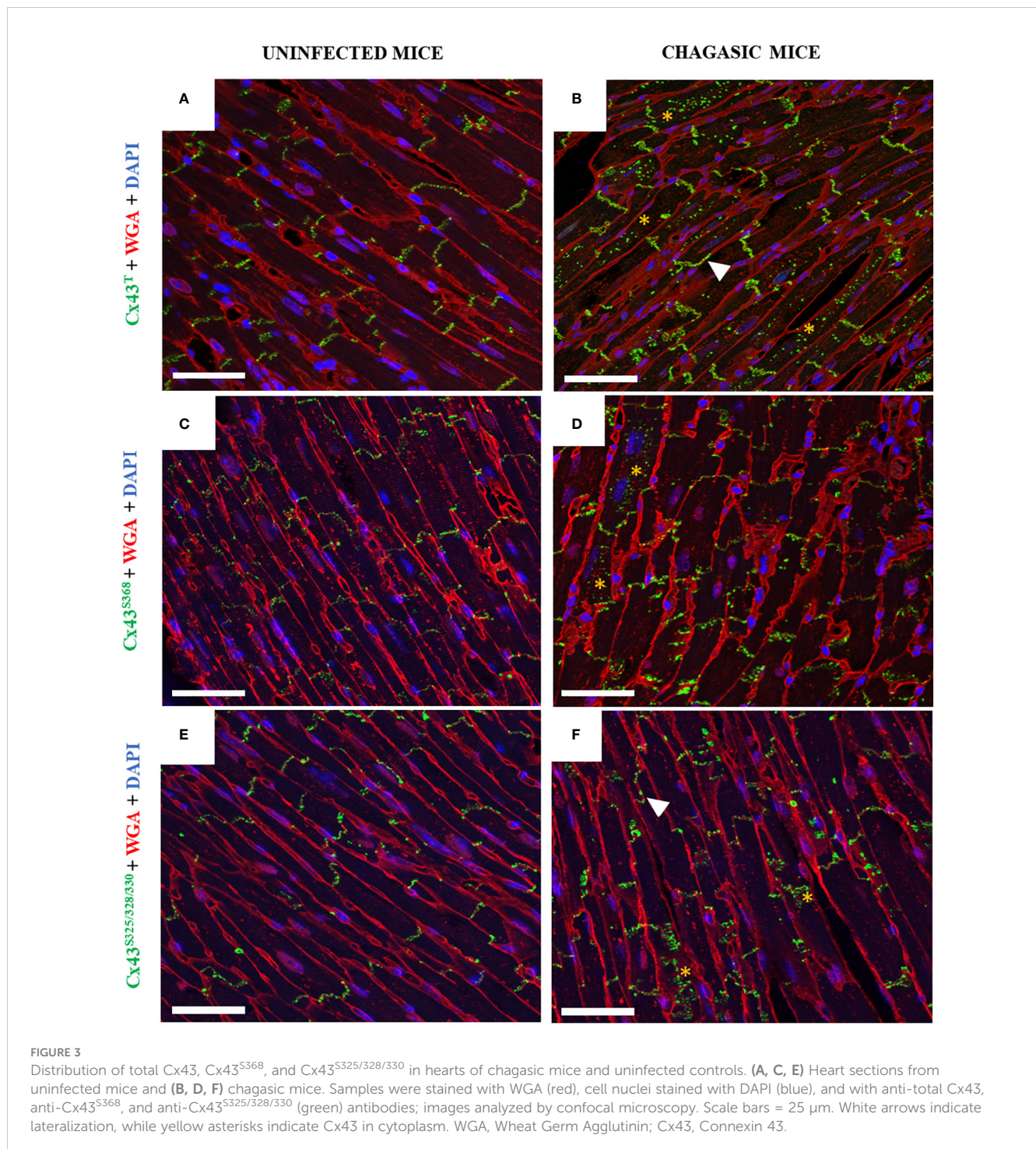
FIGURE 2
Morphological analysis and gene expression of pro-inflammatory cytokines in the hearts of uninfected and chagasic mice at 6 and 12 months after infection. **(A, B)** Representative micrographs of hematoxylin and eosin-stained heart sections of uninfected and chagasic mice at 12 months following infection. **(C)** Inflammatory cells quantified by morphometric analysis. **(D, E)** Micrographs of picrosirius red-stained heart sections of uninfected and chagasic mice. **(F)** Fibrotic area represented by percentage of collagen deposition in heart sections. Gene expression of pro-inflammatory cytokines **(G)** *Tnf*, **(H)** *Il1b*, **(I)** *Ifng*, and **(J)** *Gja1* assessed by RT-qPCR using cDNA samples prepared from mRNA extracted from experimental mouse hearts. Values represent means $\pm$ S.E.M. of 5-6 mice per group. ***$P< 0.001$; **$P< 0.01$; *$P<0.05$ compared to uninfected group.

were also evaluated for the distribution of Cx43^{T}, Cx43^{S368}, and Cx43$^{S325/328/330}$. In a healthy heart sample, Cx43^{T} staining was predominantly localized in cardiomyocyte intercalated discs (Figure 6A). By contrast, Cx43^{T} localization was altered in the Chagasic hearts, as evidenced by expression in lateral membranes as well as the cytoplasm (Figure 6B). Using an antibody specific for Cx43^{S368}, weak staining was observed in the healthy heart (Figure 6C) compared to intense labeling in chagasic heart sections, mainly localized in the lateral membranes and cardiomyocyte cytoplasm (Figure 6D). Similar results were obtained with antibodies against Cx43$^{S325/328/330}$ (Figures 6E, F). Double-staining with Cx43^{T} and N-cadherin revealed the expression of both Cx43^{T} and N-cadherin in the intercalated discs of the control heart sample (Figure 6G). However, in chagasic hearts, less intense co-staining of Cx43^{T} and N-cadherin was seen in the intercalated disc areas, with scattered Cx43^{T} staining observed in regions adjacent to the intercalated discs (Figure 6H).

A pro-inflammatory microenvironment induces alterations in Cx43 distribution, reduces dye transfer capacity, and reduces action potential duration in cardiomyocytes *in vitro*

IPSC-derived cardiomyocytes and H9c2 cells were stimulated *in vitro* with pro-inflammatory cytokines (IL-1β, TNF, IFN-γ) to simulate the inflammatory microenvironment found in chagasic hearts (Figure 7A). Confocal microscopy analysis revealed marked alterations in Cx43 distribution in both cell cultures, with staining spread throughout the cytoplasm of cardiomyocytes in contrast to non-stimulated cells, in which this protein was mainly localized in the plasma membrane region (Figure 7B). Immunofluorescence in H9c2 cells and iPSC-derived cardiomyocytes indicated perinuclear and dispersed Cx43 staining throughout the cytoplasm in cells stimulated with pro-inflammatory cytokines, while non-stimulated

FIGURE 3
Distribution of total Cx43, Cx43^{S368}, and Cx43$^{S325/328/330}$ in hearts of chagasic mice and uninfected controls. **(A, C, E)** Heart sections from uninfected mice and **(B, D, F)** chagasic mice. Samples were stained with WGA (red), cell nuclei stained with DAPI (blue), and with anti-total Cx43, anti-Cx43^{S368}, and anti-Cx43$^{S325/328/330}$ (green) antibodies; images analyzed by confocal microscopy. Scale bars = 25 μm. White arrows indicate lateralization, while yellow asterisks indicate Cx43 in cytoplasm. WGA, Wheat Germ Agglutinin; Cx43, Connexin 43.

cells showed higher Cx43 fluorescence intensity in cell membranes that frequently coincided with N-cadherin staining (Figure 7C).

Functional analyses were performed *in vitro* to evaluate the influence of an inflammatory microenvironment on action potential duration in human iPSC-derived cardiomyocytes and dye transfer between adjacent cells in H9c2 cells (Figure 8A). IPSC-derived cardiomyocytes stimulated for 24 or 48 hours with a combination of pro-inflammatory cytokines showed significant reductions in APD at different repolarization points (10, 50, and 90%) compared to control cells, with a marked further reduction resulting from longer stimulation (Figure 8B). Finally, the extent of lucifer yellow dye transfer was assessed in H9c2 cells, revealing less diffusion of dye in stimulated cells compared to unstimulated control cells (Figure 8C). Dye diffusion was quantified by measuring the stained area, confirming a statistically significant difference (unstimulated cardiomyocytes: 511.8 ± 223.3 mm^2, compared to 248.8 ± 122.9 mm^2 in cytokine-stimulated cardiomyocytes; p = 0.015).
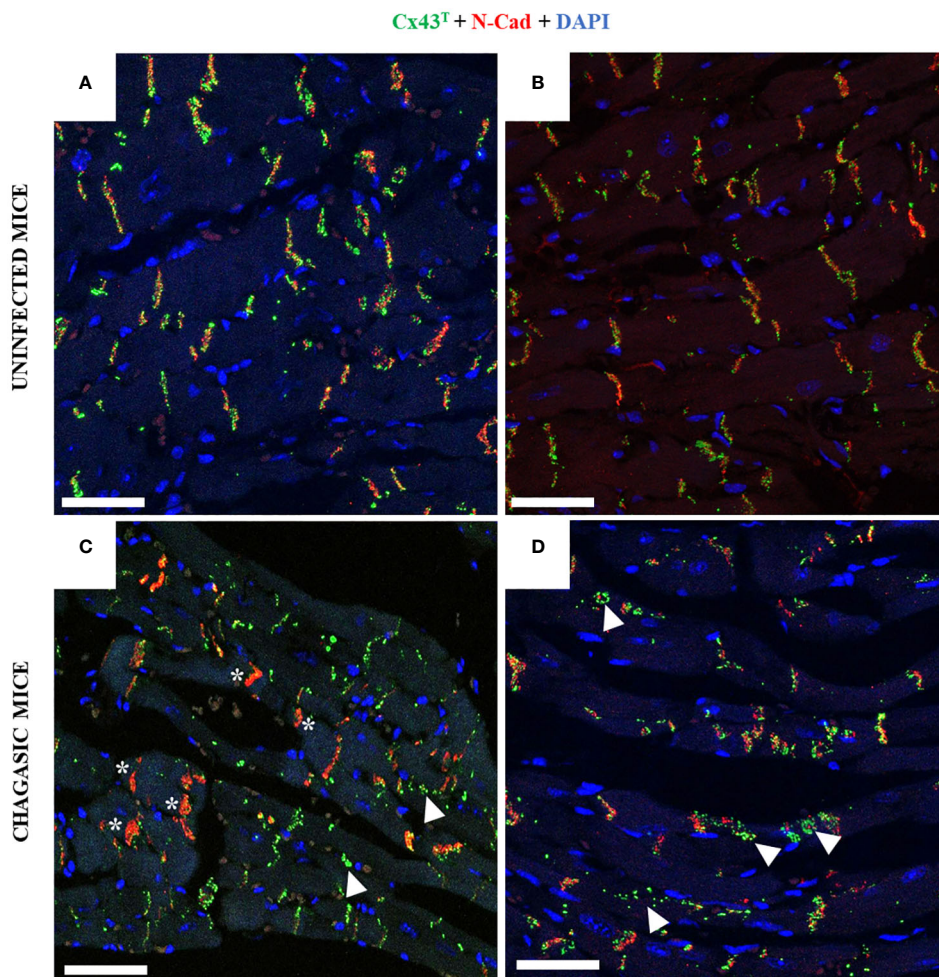
FIGURE 4

Co-staining with Cx43 and N-Cadherin in hearts of chagasic mice and uninfected controls. **(A, B)** Non-infected hearts show the presence of Cx43 (green) and N-cadherin (red) in the intercalated disk area; **(C, D)** chagasic hearts frequently presented N-cad exclusively in intercalated disc areas, with Cx43 dispersed into the cytoplasm. White arrows indicate Cx43 in cytoplasm, while white asterisks indicate intercalated discs with only N-cad expression. N-cad, N-cadherin; Cx43, Connexin 43. Scale bars = 25 μm.

Discussion

Under pathological conditions, cardiomyocyte Cx43 localization can change, contributing to improper electrical potential conduction within the heart (14, 16, 23, 30). The present study investigated alterations in conduction and correlated it with Cx43 localization in CCC. Our results indicate that CCC is associated with marked alterations in Cx43 distribution and phosphorylation patterns in an experimental mouse CCC model. Importantly, our analysis of human heart samples obtained from end-stage CCC subjects revealed similar alterations in Cx43 distribution. Moreover, *in vitro* experimentation mimicking the inflammatory microenvironment found in CCC also induced alterations in Cx43 distribution in both human and murine cardiomyocytes, as well as impaired intercellular communication through gap junctions. Taken together, these results reinforce the role played by inflammation in promoting structural and functional cardiac alterations, as well as highlighting

the potential of immunomodulation as a potential strategy for the treatment of CCC (31).

Mice with CCC exhibited impaired cardiac function, as evidenced by electrical conduction disturbances, which is consistent with previous studies employing a similar experimental approach (20, 21, 32). Our EKG analysis revealed different degrees of arrhythmias in animals with CCC, which is also convergent with previous reports (20, 32, 33). Additionally, mice with CCC exhibited a reduced ability to run on a treadmill, which could be associated with a compromised cardiac function (20, 32), as well as skeletal muscle alterations, since chronic *T. cruzi* infection is also characterized by intense myositis (34).

Intense inflammation and fibrosis, hallmarks of chronic Chagas cardiomyopathy, were identified in the hearts of chronically infected mice, similarly to reports in previous studies (20, 21, 32). Both processes may contribute to the development of the conduction disturbances observed in our model. Fibrosis deposition constitutes an important factor in the genesis of
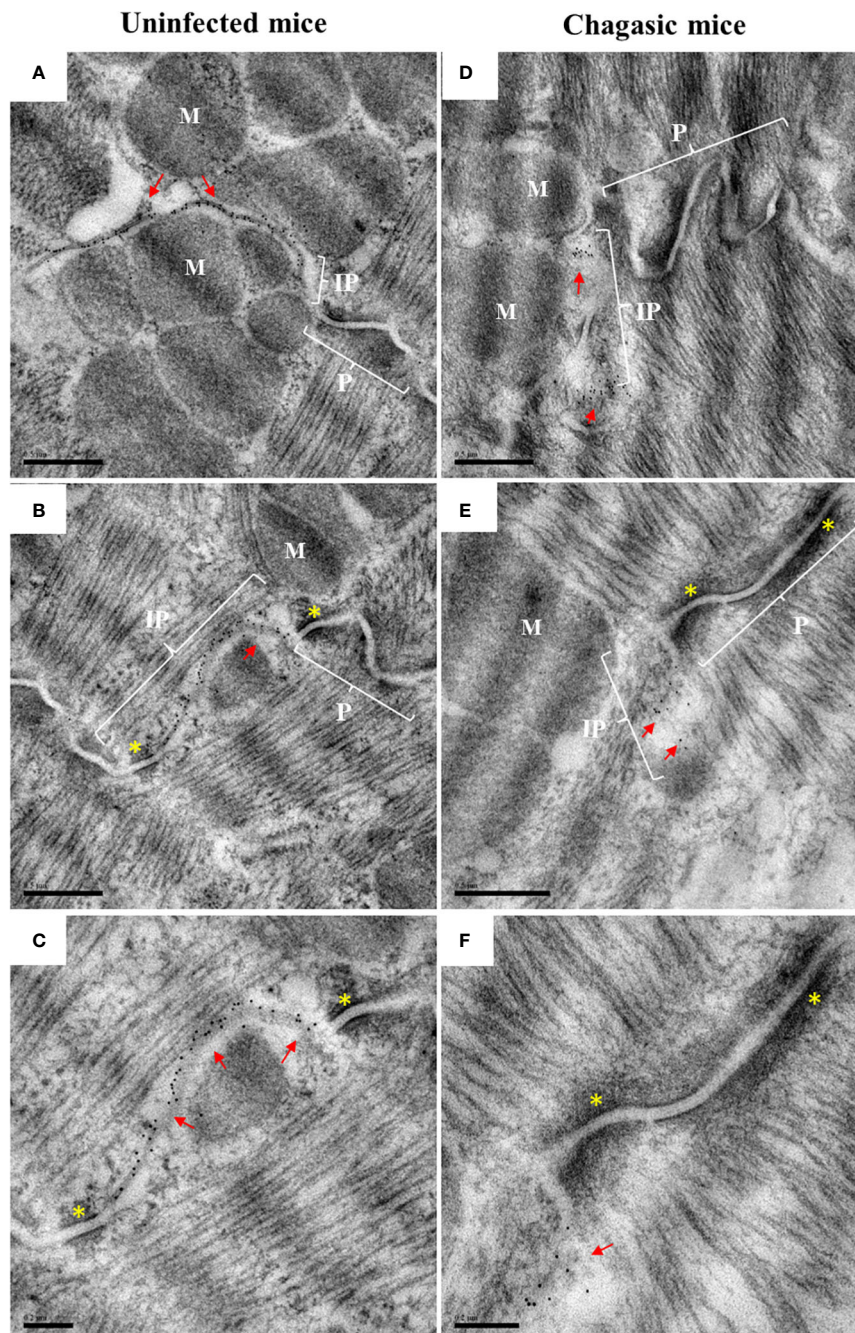
FIGURE 5
Ultrastructural analysis of total Cx43 in intercalated discs. Hearts from uninfected and chagasic control mice (n = 3 per group) were processed for analysis by transmission electron microscopy. Ultrathin sections were incubated with total anti-Cx43 antibody, with labeling revealed by the immunogold technique. **(A–C)** representative sections from uninfected control mice; **(D–F)** representative sections from chagasic mice. Red arrows indicate the presence of gap junctions in the intercalated discs; yellow asterisks indicate desmosome; P, plicate; IP, interplicate; M, myofibrils. Scale bars = 0.5 μm **(A, B, D, E)**, 0.2 μm **(C, F)**.

arrhythmias, suppressing the propagation of cardiac action potential (35). At the same time, a persistent inflammatory process leads not only to the loss of myofibers and the replacement of contractile fibers with fibrosis, but is also responsible for neuronal destruction of the autonomic nervous system that may contribute to the genesis of conduction disturbances (36).

Phosphorylation at different serine and/or tyrosine residues in the C-terminal domain of Cx43 plays an important role in the regulation of this protein's biological activity, causing electrical decoupling in the heart, which may lead to reentry circuits and enable the onset of ventricular arrhythmias (5, 6, 37–39). Here, we observed alterations in the localization of Cx43^{T}, Cx43^{S368}, Cx43$^{S325/328/330}$ in both the experimental animal model as well as in human hearts. Altered
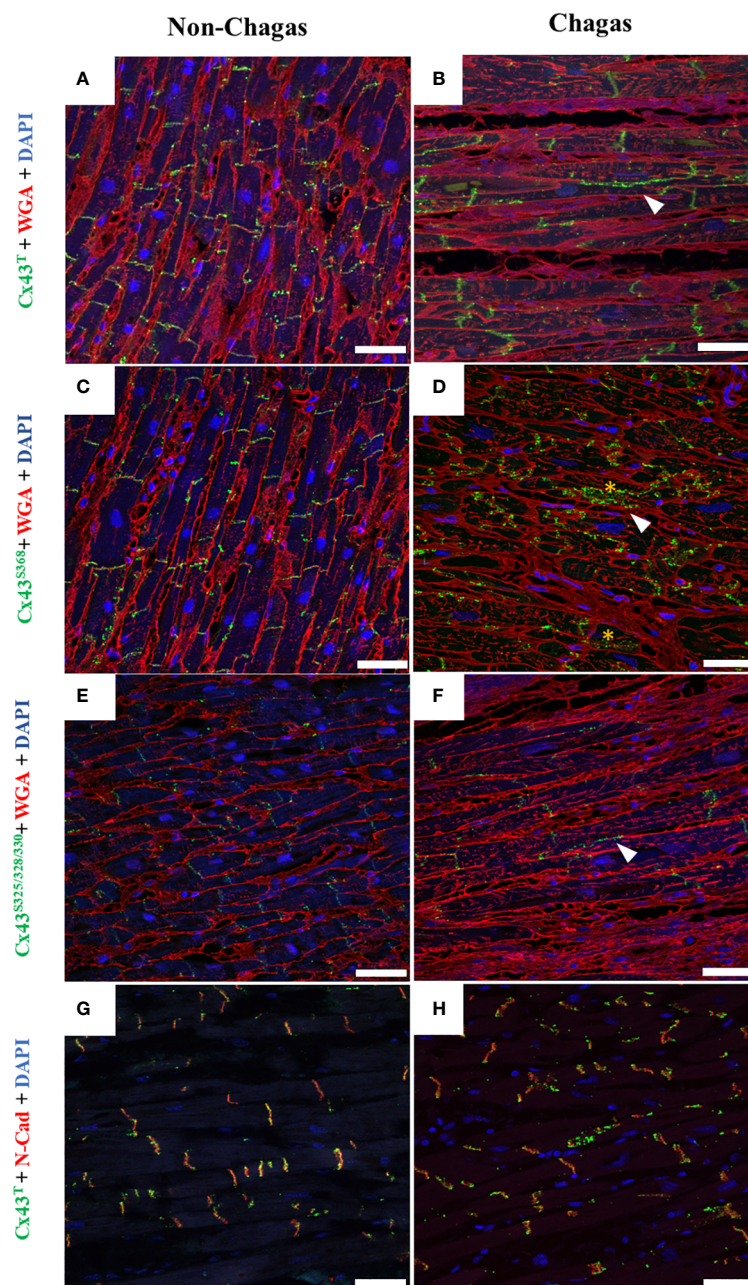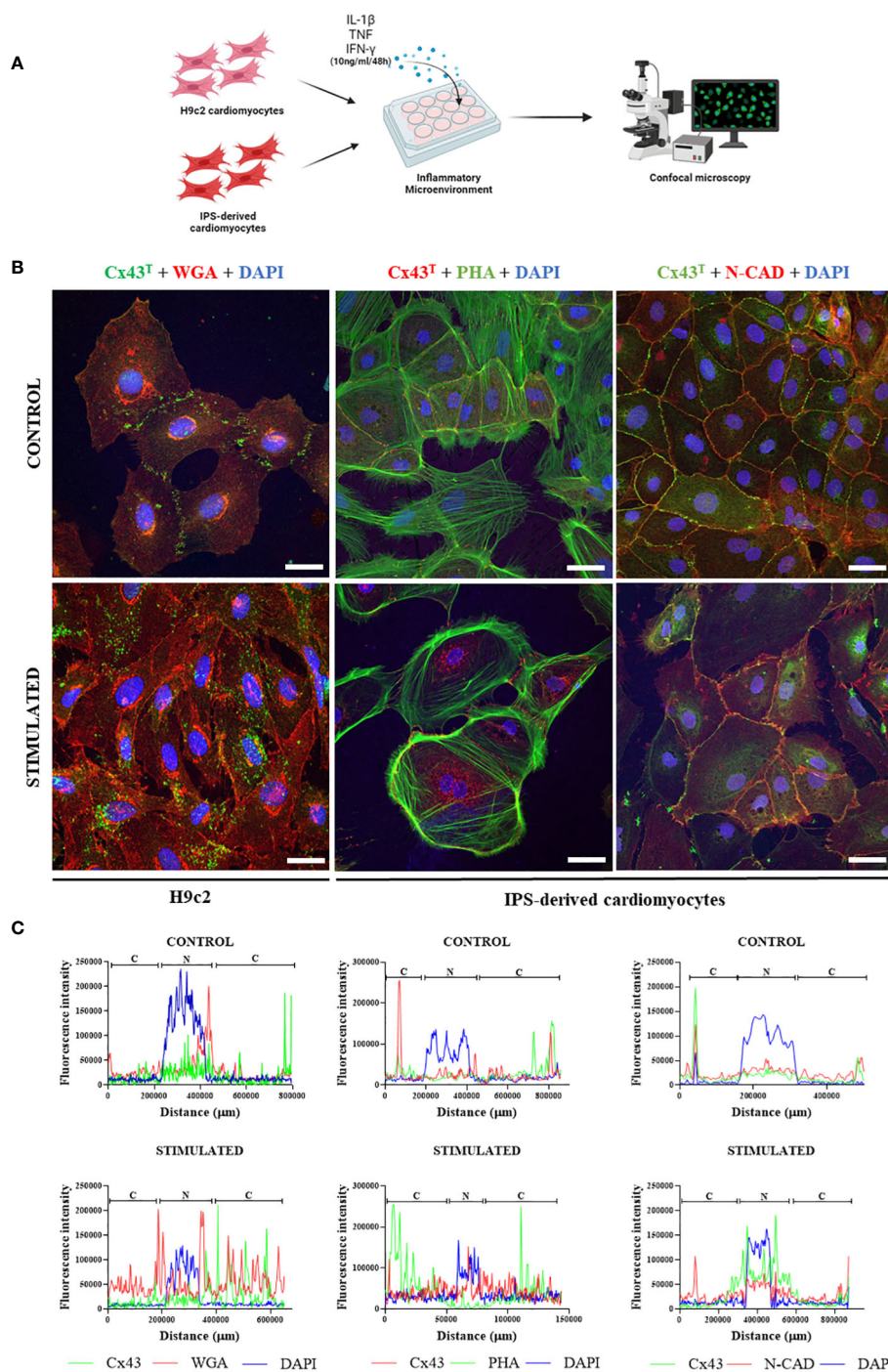
FIGURE 6
Distribution of total Cx43, Cx43^{S368}, and Cx43$^{S325/328/330}$ in human cardiac muscle tissue. **(A, C, E)** Sections of explanted hearts from non-Chagas patients and **(B, D, F)** sections of explanted hearts from Chagas patients who underwent heart transplantation were analyzed by immunofluorescence. Samples were labeled with WGA (red), cell nuclei with DAPI (blue), and total Cx43 total, Cx43^{S368} or Cx43$^{S325/328/330}$ (green). **(G, H)** Co-labeling of Cx43 (green) and N-cadherin (red), and co-localization between Cx43 and N-cadherin (yellow). White arrows indicate the presence of Cx43 outside the intercalated disc area. Scale bars = 50 μm. WGA, Wheat Germ Agglutinin; N-cad, N-cadherin; Cx43, Connexin 43.

staining patterns for Cx43 isoforms were observed in the lateral membrane and internalized in the cytoplasm of cardiac cells. Previous studies have shown that the localization of Cx43 outside the intercalated disks reduces the speed of the action potential propagation (40). Conversely, in the hearts of uninfected mice, Cx43 was predominantly localized in the intercalated discs, which is indicative of effective "cell-cell" conduction of electrical potential between neighboring cardiomyocytes (15, 41–43). The increased phosphorylation of Cx43^{S368} is known to reduce permeability and

promote lateralization and internalization of communicating channels, a phenomenon observed in experimental models of cardiac ischemia (18, 44, 45). Moreover, Lampe et al. (2006) suggested that the dephosphorylation of Cx43$^{S325/328/330}$ plays an important role in compromising permeability in gap junctions, reducing communication between cardiomyocytes, in the context of heart disease, which may also be occurring in CCC.

Inflammation is known to induce alterations in the gap junctions formed by Cx43 by impairing protein expression and

FIGURE 7
Effect of inflammatory microenvironment on Cx43 distribution *in vitro*. **(A)** Experimental *in vitro* design involving H9c2 cells and iPSC-derived cardiomyocytes, with both cell types stimulated by pro-inflammatory cytokines (IL-1β, TNF, and IFN-γ, 10 ng/ml of each cytokine) for 48 hours for immunofluorescence analysis. **(B)** Immunofluorescence of H9c2 cells and iPSC-derived cardiomyocytes; **(C)** Analysis of Cx43 distribution by fluorescence intensity in H9c2 cells and iPSC-derived cardiomyocytes after 48 hours of stimulation with pro-inflammatory cytokines IL-1β, TNF, and IFN-γ. Cells were stained with WGA (red), cell nuclei with DAPI (blue), and total Cx43 with anti-Cx43 antibody (green). Images analyzed by confocal microscopy. Scale bars = 50 μm. WGA, Wheat Germ Agglutinin; Cx43, Connexin 43; IL-1β, Interleukin 1 beta; TNF, Tumor necrosis factor; IFN-γ, Interferon gamma; C, Cytoplasm; N, Cell Nucleus. Created with BioRender.com.

localization (5, 20, 21). Elevated levels of pro-inflammatory cytokines, such as TNF, IL-1β, and IFN-γ, have been shown to promote alterations in Cx43 expression (15, 27, 46–48), as well as increase Cx43^{S368} phosphorylation by activating different signaling

pathways (7, 13, 15, 18, 46, 49). These observations underscore the significance of our findings in this study, in which increased expression of genes encoding cytokines IL-1β, TNF and IFN-γ was observed in the hearts of mice with CCC. The correlation
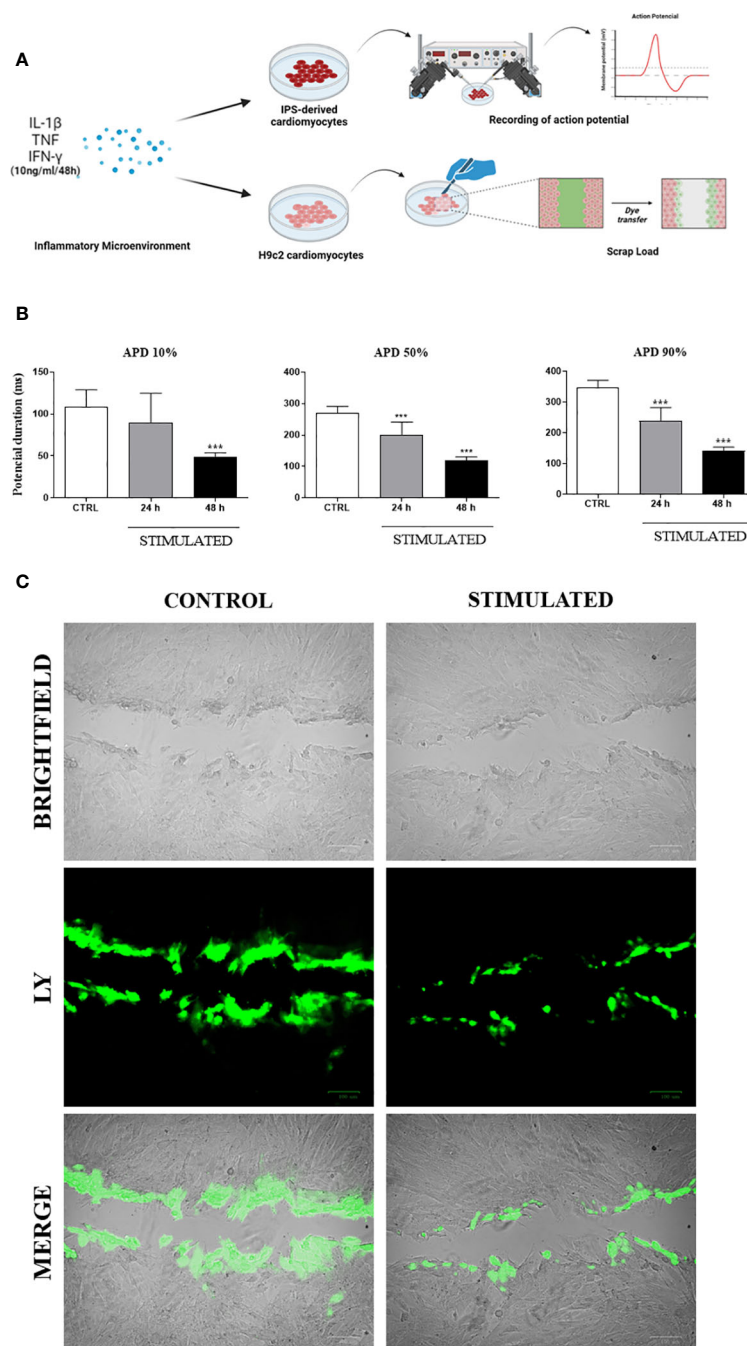
FIGURE 8

Functional *in vitro* analysis of Cx43: Action Potential Duration and Lucifer Yellow dye transfer. **(A)** Schematic drawing of functional testing performed on iPSC-derived cardiomyocytes and H9c2 cardiomyocytes, stimulated with pro-inflammatory cytokines to respectively analyze the duration of action potential and dye transfer between neighboring cells. **(B)** After stimulation, action potential duration (APD) of iPSC-derived cardiomyocytes was determined at 10%, 50% and 90% levels. **(C)** Lucifer Yellow dye transfer test (green) performed in H9c2 cells (bright field) stimulated with pro-inflammatory cytokines IL-1β, TNF, and IFN-γ for 48 hours. Predominance of dye observed in cells at the margin where scalpel incision was made, while absence of stimulation resulted in dye reaching more distant cells; IL-1β = Interleukin 1 beta; TNF = Tumor necrosis factor; IFN-γ = Interferon gamma; CTRL = Control group; ***P< 0.001 compared to unstimulated cells. Scale bars = 100 μm.

between inflammatory cytokine production and changes in Cx43 phosphorylation and localization observed in our study further highlights the intricate interplay between inflammation and cardiac electrical coupling in the context of CCC.

Alterations in intercalated disc structure influence the regulation of cardiac conduction and are associated with pathological conditions (50). To better investigate the distribution of Cx43 in intercalated discs, we performed co-staining with an antibody against N-cadherin (a protein present in intercalated discs) along with Cx43. This analysis revealed scarce staining for Cx43 in the intercalated discs of chagasic heart sections, whereas uninfected mice exhibited more uniform and correlated staining for

N-cadherin and Cx43 in the intercalated discs. This alteration in distribution pattern aligns with findings reported by Himelman and colleagues in a model of Duchenne muscular dystrophy (23). Alterations in Cx43 distribution were further confirmed by transmission electron microscopy, which demonstrated the localization of Cx43 in the interplicate regions of intercalated discs, as well as frequent labeling in concentric ring structures, which is suggestive of alterations in gap junctions containing membranes during internalization. Similar ultrastructural alterations were also reported by Hesketh and collaborators (2010), who evaluated Cx43 distribution in canine models of heart failure (41).

The present study observed significantly lower expression of the gene that encodes Cx43 (*Gja1*) in mice at six months after infection, similarly to previous studies reporting the downregulation of Cx43 in the heart (45, 51). However, at 12 months after infection, higher *Gja1* expression was noted, which may indicate the presence of a compensatory mechanism in response to the cardiac damage caused during disease progression (51). Further analysis will be necessary to fully clarify the long-term regulation of Cx43 gene expression within the context of CCC.

To further elucidate the influence of inflammation on Cx43 expression and function, we simulated an inflammatory microenvironment in cultures of human iPSC-derived cardiomyocytes and H9c2 cells by incubation with a pool of pro-inflammatory cytokines (IL-1β, TNF and IFN-γ). After 48 hours of stimulation, a reduction in the duration of action potential in iPSC-derived cardiomyocytes was noted, as well as the decreased ability of H9c2 cells to transfer LY dye between neighboring cells and greater Cx43 dispersion throughout the cytoplasm in both cell types investigated. Previous studies demonstrated that *T. cruzi*-infected cardiomyocytes lose the ability to transfer LY dye to adjacent cells (9, 48, 52–54). Taken together, our results indicate that the persistence of a pro-inflammatory microenvironment due to scarce residual parasitism during the chronic phase of infection may also play a major role in Cx43 disorganization (10, 12, 55), as well as contribute to the conduction disturbances seen in CCC.

In conclusion, the pro-inflammatory milieu associated with CCC provokes a marked impairment in Cx43 distribution and cardiac function. The present findings suggest possibilities for further investigations to seek a deeper understanding of the signaling pathways that may be activated by pro-inflammatory cytokines, resulting in the dysregulation of Cx43. Additionally, we highlight the importance of exploring potential therapeutic targets that could improve Cx43 function and prevent the development of serious arrhythmias in patients with CCC.

Data availability statement

The raw data supporting the conclusions of this article will be made available by the authors, without undue reservation.

Ethics statement

The studies involving humans were approved by the National Ethical Review Board in Brazil (CONEP). The studies were conducted in accordance with the local legislation and institutional requirements. The participants provided their written informed consent to participate in this study. The animal study was approved by Animal Use Ethics Committee of the São Rafael Hospital and the Gonçalo Moniz Institute. The study was conducted in accordance with the local legislation and institutional requirements.

Author contributions

BB: Conceptualization, Data curation, Formal analysis, Investigation, Methodology, Writing – original draft, Writing – review & editing. MN: Data curation, Formal analysis, Methodology, Writing – original draft. CC: Formal analysis, Methodology, Writing – original draft, Data curation. CM: Conceptualization, Data curation, Formal analysis, Writing – original draft, Writing – review & editing, Methodology. PD: Data curation, Formal analysis, Methodology, Writing – original draft. CF: Data curation, Formal analysis, Methodology, Writing – original draft. GS: Formal analysis, Methodology, Writing – original draft, Data curation. DS: Formal analysis, Methodology, Writing – original draft, Data curation. FT: Formal analysis, Methodology, Writing – original draft. JN: Formal analysis, Methodology, Writing – original draft. SM: Conceptualization, Data curation, Formal analysis, Investigation, Methodology, Writing – original draft. PL: Formal analysis, Methodology, Writing – original draft. KC: Formal analysis, Methodology, Writing – original draft, Data curation. TKB: Formal analysis, Methodology, Writing – original draft, Data curation. RR: Conceptualization, Formal analysis, Funding acquisition, Supervision, Writing – original draft. AC: Conceptualization, Formal analysis, Funding acquisition, Project administration, Supervision, Writing – original draft, Writing – review & editing. MS: Conceptualization, Data curation, Formal analysis, Funding acquisition, Project administration, Supervision, Writing – original draft, Writing – review & editing.

Funding

Conflict of interest

The authors declare that the research was conducted in the absence of any commercial or financial relationships that could be construed as a potential conflict of interest.

Publisher's note

All claims expressed in this article are solely those of the authors and do not necessarily represent those of their affiliated organizations, or those of the publisher, the editors and the reviewers. Any product that may be evaluated in this article, or claim that may be made by its manufacturer, is not guaranteed or endorsed by the publisher.

Supplementary material

The Supplementary Material for this article can be found online at: https://www.frontiersin.org/articles/10.3389/fimmu.2024.1440662/full#supplementary-material

References

1. Chagas disease (American trypanosomiasis). Available online at: https://www.who.int/health-topics/chagas-disease (Accessed September 10, 2023).

2. Coura JR, Borges-Pereira J. Chagas disease: 100 years after its discovery. *A systemic review. Acta Tropica*. (2010) 115:5–13. doi: 10.1016/j.actatropica.2010.03.008

3. Benziger CP, do Carmo GAL, Ribeiro ALP. Chagas cardiomyopathy: Clinical presentation and management in the Americas. *Cardiol Clinics*. (2017) 35:31–47. doi: 10.1016/j.ccl.2016.08.013

4. Simões MV, Romano MMD, Schmidt A, Martins KSM, Marin-Neto JA. Chagas disease cardiomyopathy. *Int J Cardiovasc Sci*. (2018) 31:173–89. doi: 10.5935/2359-4802.20180011

5. Barbosa MPT, do Carmo AAL, Rocha MOC, Ribeiro ALP. Ventricular arrhythmias in Chagas disease. *Rev da Sociedade Bras Medicina Trop*. (2015) 48:4–10. doi: 10.1590/0037-8682-0003-2014

6. Kumar V. Ventricular arrhythmias in chronic Chagas cardiomyopathy: Can studying myocardial sympathetic denervation provide the answers? *J Nucl Cardiol*. (2016) 25:84–5. doi: 10.1007/s12350-016-0587-z

7. Axelsen LN, Calloe K, Holstein-Rathlou N-H, Nielsen MS. Managing the complexity of communication: regulation of gap junctions by post-translational modification. *Front Pharmacol*. (2013) 4:130. doi: 10.3389/fphar.2013.00130

8. Duffy HS, Fort AG, Spray DC. Cardiac connexins: Genes to nexus. *Adv Cardiol*. (2006) 42:1–17. doi: 10.1159/000092550

9. Adesse D, Goldenberg RC, Fortes FS, Jasmin, Iacobas DA, Iacobas S, et al. Gap junctions and chagas disease. *Natl Institutes Health*. (2011) 76:63–81. doi: 10.1038/jid.2014.371

10. Adesse D, Garzoni LR, Huang H, Tanowitz HB, De M, Meirelles N, et al. *Trypanosoma cruzi* induces changes in cardiac connexin43 expression. *Microbes Infect*. (2008) 10:21–8. doi: 10.1016/j.micinf.2007.09.017.Trypanosoma

11. de Carvalho AC, Tanowitz HB, Wittner M, Dermietzel R, Roy C, Hertzberg EL, et al. Gap junction distribution is altered between cardiac myocytes infected with *Trypanosoma cruzi. Circ Res*. (1992) 70:733–42. doi: 10.1161/01.RES.70.4.733

12. De Carvalho ACC, Masuda MO, Tanowitz HB, Wittner M, Goldenberg RCS, Spray DC. Conduction defects and arrhythmias in chagas' Disease: possible role of gap junctions and humoral mechanisms. *J Cardiovasc Electrophysiology*. (1994) 5:686–98. doi: 10.1111/j.1540-8167.1994.tb01191.x

13. Lampe PD, TenBroek EM, Burt JM, Kurata WE, Johnson RG, Lau AF. Phosphorylation of connexin43 on serine368 by protein kinase C regulates gap junctional communication. *J Cell Biol*. (2000) 149:1503–12. doi: 10.1083/jcb.149.7.1503

14. Solan JL, Lampe PD. Key connexin 43 phosphorylation events regulate the gap junction life cycle. *J Membrane Biol*. (2007) 217:35–41. doi: 10.1007/s00232-007-9035-y

15. Zhong C, Chang H, Wu Y, Zhou L, Wang Y, Wang M, et al. Up-regulated Cx43 phosphorylation at Ser368 prolongs QRS duration in myocarditis. *J Cell Mol Med*. (2018) 22:3537–47. doi: 10.1111/jcmm.13631

16. Lampe PD, Copper CD, King TJ, Burt JM. Analysis of Connexin43 phosphorylated at S325, S328 and S330 in normoxic and ischemic heart. *J Cell Sci*. (2006) 119:3435–42. doi: 10.1242/jcs.03089

17. Palatinus JA, Rhett JM, Gourdie RG. The connexin43 carboxyl terminus and cardiac gap junction organization. *Biochim Biophys Acta - Biomembranes*. (2012) 1818:1831–43. doi: 10.1016/j.bbamem.2011.08.006

18. Solan JL, Lampe PD. Specific Cx43 phosphorylation events regulate gap junction turnover *in vivo*. *FEBS Lett*. (2014) 23:1423–9. doi: 10.1016/j.febslet.2014.01.049

19. Brener Z. Therapeutic activity and criterion of cure on mice experimentally infected with *Trypanosoma cruzi. Rev Inst Med Trop Sao Paulo*. (1962) 4:389–96.

20. Macambira SG, Vasconcelos JF, Costa CRS, Klein W, Lima RS, Guimarães P, et al. Granulocyte colony-stimulating factor treatment in chronic Chagas disease:

21. Vasconcelos JF, Souza BSF, Lins TFS, Garcia LMS, Kaneto CM, Sampaio GP, et al. Administration of granulocyte colony-stimulating factor induces immunomodulation, recruitment of T regulatory cells, reduction of myocarditis and decrease of parasite load in a mouse model of chronic Chagas disease cardiomyopathy. *FASEB J*. (2013) 27:4691–702. doi: 10.1096/fj.13-229351

22. Schmittgen TD, Livak KJ. Analyzing real-time PCR data by the comparative CT method. *Nat Protoc*. (2008) 3:1101–8. doi: 10.1038/nprot.2008.73

23. Himelman E, Lillo MA, Nouet J, Patrick Gonzalez J, Zhao Q, Xie LH, et al. Prevention of connexin-43 remodeling protects against Duchenne muscular dystrophy cardiomyopathy. *J Clin Invest*. (2020) 130:1713–27. doi: 10.1172/JCI128190

24. Wenisch S, Ada Cavalcanti-Adam E, Tryankowski E, Raabe O, Kilian O, Heiss C, et al. Light- and transmission-electron-microscopic investigations on distribution of CD44, connexin 43 and actin cytoskeleton during the foreign body reaction to a nanoparticular hydroxyapatite in mini-pigs. *Acta Biomaterialia*. (2012) 8:2807–14. doi: 10.1016/j.actbio.2012.03.039

25. Branco AF, Pereira SP, Gonzalez S, Gusev O, Rizvanov AA, Oliveira PJ. Gene expression profiling of H9c2 myoblast differentiation towards a cardiac-like phenotype. *PLoS One*. (2015) 10:e0129303. doi: 10.1371/journal.pone.0129303

26. Nunes JPS, Andrieux P, Brochet P, Almeida RR, Kitano E, Honda AK, et al. Co-exposure of cardiomyocytes to IFN-γ and TNF-α Induces mitochondrial dysfunction and nitro-oxidative stress: Implications for the pathogenesis of chronic chagas disease cardiomyopathy. *Front Immunol*. (2021) 12:755862. doi: 10.3389/fimmu.2021.755862

27. Sáez JC, Constreras-Duarte S, Gómez GI, Labra VC, Santibañez CA, Avendaño BC, et al. Connexin 43 hemichannel activity promoted by pro-inflammatory cytokines and high glucose alters endothelial cell function. *Front Immunol*. (2018) 9:1899. doi: 10.3389/fimmu.2018.01899

28. Babica P, Sovadinová I, Upham BL. Scrape loading/dye transfer assay. *Methods Mol Biol*. (2016) 1437:133–44. doi: 10.1007/978-1-4939-3664-9_9

29. Kasai-Brunswick TH, Silva dos Santos D, Ferreira RP, Araujo DS, Dias GM, Coutinho JLA, et al. Generation of patient-specific induced pluripotent stem cell lines from one patient with Jervell and Lange-Nielsen syndrome, one with type 1 long QT syndrome and two healthy relatives. *Stem Cell Res*. (2018) 31:174–80. doi: 10.1016/j.scr.2018.07.016

30. Sosinsky GE, Solan JL, Gaietta GM, Ngan L, Lee GJ, Mackey MR, et al. The C-terminus of connexin43 adopts different conformations in the Golgi and gap junction as detected with structure-specific antibodies. *Biochem J*. (2008) 408:375–85. doi: 10.1042/BJ20070550

31. de Souza Santos E, Keyse Carvalho Silva D, Padilha Zurita Claro dos Reis B, Cardim Barreto B, MaChado Azevedo Cardoso C, Ribeiro dos Santos R, et al. Immunomodulation for the treatment of chronic chagas disease cardiomyopathy: A new approach to an old enemy. *Front Cell infection Microbiol*. (2021) 11:765879. doi: 10.3389/fcimb.2021.765879

32. Meira CS, De Souza Santos E, Do Espírito Santo RF, Vasconcelos JF, Orge ID, Nonaka CKV, et al. Betulinic acid derivative BA5, attenuates inflammation and fibrosis in experimental chronic Chagas disease cardiomyopathy by inducing IL-10 and M2 polarization. *Front Immunol*. (2019) 10:1257. doi: 10.3389/fimmu.2019.01257

33. Vasconcelos JF, Meira CS, Silva DN, Nonaka CKV, Daltro PS, MacAmbira SG, et al. Therapeutic effects of sphingosine kinase inhibitor N,N-dimethylsphingosine (DMS) in experimental chronic Chagas disease cardiomyopathy. *Sci Rep*. (2017) 7:1–14. doi: 10.1038/s41598-017-06275-z

34. Solana ME, Ferrer MF, Novoa MM, Song WC, Gómez RM. Decay-accelerating factor 1 deficiency exacerbates *Trypanosoma cruzi*-induced murine chronic myositis. *Muscle Nerve*. (2012) 46:582–7. doi: 10.1002/mus.23347

preservation and improvement of cardiac structure and function. *FASEB J*. (2009) 23:3843–50. doi: 10.1096/fj.09-137869

35. Oliviero F, Diwan V, Radeke HH, Peiró C, Es CP, Sánchez-Ferrer CF, et al. IL-1β Inhibition in cardiovascular complications associated to diabetes mellitus. *Front Pharmacol*. (2017) 8:363. doi: 10.3389/fphar.2017.00363

36. Rassi A, Rassi A, Marin-Neto JA. Chagas heart disease: pathophysiologic mechanisms, prognostic factors and risk stratification. *Mem Inst Oswaldo Cruz*. (2009) 104:152–8. doi: 10.1590/S0074-02762009000900021

37. Jongsma HJ, Wilders R. Gap junctions in cardiovascular disease. *Circ Res*. (2000) 86:1193–7. doi: 10.1161/01.RES.86.12.1193

38. Michela P, Velia V, Aldo P, Ada P. Role of connexin 43 in cardiovascular diseases. *Eur J Pharmacol*. (2015) 768:71–6. doi: 10.1016/j.ejphar.2015.10.030

39. Solan JL, Lampe PD. Connexin43 phosphorylation: structural changes and biological effects. *Biochem J*. (2009) 419:261–72. doi: 10.1042/BJ20082319

40. Kleber AG, Saffitz JE. Role of the intercalated disc in cardiac propagation and arrhythmogenesis. *Front Physiol*. (2014) 5:404. doi: 10.3389/fphys.2014.00404

41. Hesketh GG, Shah MH, Halperin VL, Cooke CA, Akar FG, Yen TE, et al. Ultrastructure and regulation of lateralized connexin43 in the failing heart. *Circ Res*. (2010) 106:1153–63. doi: 10.1161/CIRCRESAHA.108.182147

42. Hesketh GG, Van Eyk JE, Tomaselli GF. Mechanisms of gap junction traffic in health and disease. *Cardiovasc Pharmacol*. (2009) 54:263–72. doi: 10.1097/FJC.0b013e3181ba0811

43. Kohutova J, Elsnicova B, Holzerova K, Neckar J, Sebesta O, Jezkova J, et al. Anti-arrhythmic cardiac phenotype elicited by chronic intermittent hypoxia is associated with alterations in connexin-43 expression, phosphorylation, and distribution. *Front Endocrinol*. (2019) 9:789. doi: 10.3389/fendo.2018.00789

44. Ek-Vitorin JF, King TJ, Heyman NS, Lampe PD, Burt JM. Selectivity of Cx43 channels is regulated through PKC-dependent phosphorylation. *Circ Res*. (2006) 98:1498–505. doi: 10.1161/01.RES.0000227572.45891.2c

45. Zhang M, Wang Z-Z, Chen N-H. Connexin 43 phosphorylation: implications in multiple diseases. *Molecules*. (2023) 28:4914. doi: 10.3390/molecules28134914

46. Fernandez-Cobo M, Gingalewski C, Drujan D, De Maio A. Downregulation of connexin 43 gene expression in rat heart during inflammation. *role tumour necrosis factor. Cytokine*. (1999) 11:216–24. doi: 10.1006/cyto.1998.0422

47. Sáez JC, Contreras-Duarte S, Labra VC, Santibañez CA, Mellado LA, Inostroza CA, et al. Interferon-γ and high glucose-induced opening of Cx43 hemichannels causes endothelial cell dysfunction and damage. *Biochim Biophys Acta - Mol Cell Res*. (2020) 1867:118720. doi: 10.1016/j.bbamcr.2020.118720

48. Francis Stuart SD, De Jesus NM, Lindsey ML, Ripplinger CM. The crossroads of inflammation, fibrosis, and arrhythmia following myocardial infarction. *J Mol Cell Cardiol*. (2016) 91:114–22. doi: 10.1016/j.yjmcc.2015.12.024

49. Ribeiro-Rodrigues TM, Martins-Marques T, Morel S, Kwak BR, Girão H. Role of connexin 43 in different forms of intercellular communication – gap junctions, extracellular vesicles and tunnelling nanotubes. *J Cell Sci*. (2017) 130:3619–30. doi: 10.1242/jcs.200667

50. Moise N, Struckman HL, Dagher C, Veeraraghavan R, Weinberg SH. Intercalated disk nanoscale structure regulates cardiac conduction. *J Gen Physiol*. (2021) 153:e202112897. doi: 10.1085/jgp.202112897

51. Fontes MSC, Van Veen TAB, De Bakker JMT, Van Rijen HVM. Functional consequences of abnormal Cx43 expression in the heart. *Biochim Biophys Acta - Biomembranes*. (2012) 1818:2020–9. doi: 10.1016/j.bbamem.2011.07.039

52. Meng J, Xu K, Qin Y, Liu Y, Xu L, Qiao S, et al. Tumor necrosis factor-alpha disrupts cx43-mediated corneal endothelial gap junction intercellular communication. *Oxid Med Cell Longevity*. (2022) 2022:1–9. doi: 10.1155/2022/4824699

53. Pinto JMB. Electrical remodeling in ischemia and infarction. *Cardiovascular Res*. (1999) 42:284–97. doi: 10.1016/S0008-6363(99)00013-9

54. Yao JA, Hussain W, Patel P, Peters NS, Boyden PA, Wit AL. Remodeling of gap junctional channel function in epicardial border zone of healing canine infarcts. *Circ Res*. (2003) 92:437–43. doi: 10.1161/01.RES.0000059301.81035.06

55. Tanowitz HB, MaChado FS, Jelicks LA, Shirani J, Campos de Carvalho AC, Spray DC, et al. Perspectives on *trypanosoma cruzi*-induced heart disease (Chagas disease). *Prog Cardiovasc Dis*. (2009) 51:524–39. doi: 10.1016/j.pcad.2009.02.001